RJC

RASĀYAN *J. Chem.*
Vol. 18 | No. 3 |1235-1242| July-September | 2025
ISSN: 0974-1496 | e-ISSN: 0976-0083 | CODEN: RJCABP
http://www.rasayanjournal.com
http://www.rasayanjournal.co.in

EXPLORING THE MECHANISMS OF CARBON DOT-IBUPROFEN INTERACTION FOR DRUG DELIVERY APPLICATIONS: AN INTEGRATED EXPERIMENTAL AND THEORETICAL INVESTIGATION

K. Karthik[1] and S. Thangavel[2,✉]
[1]Department of Chemistry, Nandha Arts and Science College,Erode-638052, (Tamil Nadu) India
[2]Department of Chemistry, Chikkaiah Government Arts and Science College,
Erode-638004, (Tamil Nadu) India
✉Corresponding author: apstvl@gmail.com

ABSTRACT

Carbon dots (CDs) are zero-dimensional nanomaterials used for drug delivery applications due to their biocompatibility and tunable surface properties. In this study, the interaction between CD and ibuprofen (IBU) was thoroughly investigated using FTIR and UV-Vis spectroscopy, combining experimental data with density functional theory (DFT) calculations. Additionally, intrinsic bond strength and independent gradient model (IGM) analysis revealed the strength of the hydrogen bond. Furthermore, frontier molecular orbital (FMO) analysis was conducted to explore the electronic properties and reactivity of the complex, while molecular electrostatic potential (MEP) mapping highlighted the potential interaction sites. Natural bond orbital (NBO) analysis offered insights into charge transfer and stabilization energy, while the Hartree-Fock method with London dispersion corrections (HFLD) was performed to investigate the interaction energy. These findings offer valuable insights for the development of customizable and efficient carbon dot-based drug delivery systems.

Keywords: Hydrogen Bond, DFT, Ibuprofen, NBO, FMO, Drug Delivery, Carbon Dot.

RASĀYAN *J. Chem.*, Vol. 18, No.3, 2025

INTRODUCTION

CDs are zero-dimensional nanomaterials that are typically less than 10 nm in size. CD can be synthesized using top-down methods[1] and bottom-up methods.[2] Precursor materials, which range from natural biomass[1] to synthetic compounds[3]Allow CD to be highly tunable in terms of composition and functionality. CDs exhibit remarkable properties, including strong photoluminescence, high water solubility, and excellent biocompatibility.[1,3] These properties make CD useful in bioimaging[4], biosensing,[5] and drug delivery applications.[6] IBU is widely used for pain relief, arthritis, and fever reduction.[7]

Despite its widespread use, IBU has limited bioavailability due to poor solubility. Strategies to enhance its bioavailability and stability include prodrugs,[8] salt formulations,[7] co-crystallization,[9] and solid dispersion techniques. [10]Among these, co-crystallization is the most widely used technique. However, despite improvements in bioavailability, co-crystallization has some limitations, particularly in the selection of suitable co-formers. Not all co-formers are compatible with the drug or acceptable for pharmaceutical use due to concerns about toxicity and stability.[11] These limitations highlight the need for careful selection and testing of co-formers in co-crystal formulations. These limitations highlight the potential of CDs as co-formers in co-crystal formulations. CDs have proven to be non-toxic, biocompatible, and effective in improving the solubility and stability of many drugs.[12] By interacting with drug molecules, CD can enhance the solubility, stability, and controlled release of pharmaceuticals.[13] Thus, CDs are promising materials for drug formulation and delivery systems.

EXPERIMENTAL

Materials and methods

Brufen® 400 mg (ibuprofen) was obtained from Abbot, purchased from a local medical shop in Erode, Tamil Nadu. Tribulus terrestris (TT) for CD preparation was collected from the Erode district, Tamil Nadu.

Synthesis of CD and ICD

TT leaf powder (1 g) was mixed with 20 mL of distilled water and filtered. 10 mL of the resulting filtrate was heated to 185°C for 6 hours, followed by washing with 10 mL of distilled water and centrifugation at 3000 rpm for about 30 minutes to obtain carbon dots. A solution of IBU (10 mg/mL) was mixed with 5 mL of as-prepared aqueous CD and stirred at room temperature using a magnetic stirrer at 1100 rpm for 1 h. The resulting solution was used for further analysis.

Characterization

Fourier transform infrared (FTIR) spectra were obtained using a PerkinElmer Spectrum Two spectrometer. The absorption spectra were recorded using a JASCO V-750 UV-Vis spectrometer.

Computational Details

Density Functional Theory (DFT) calculations were performed using the r^{2}SCAN-3c method in ORCA software[16] to explore the molecular interactions between CD and IBU. Time-Dependent Density Functional Theory (TD-DFT) was employed to investigate electronic transitions and UV-Vis spectra, employing the CAM-B3LYP[17] functional with a Def2-TZVP basis set. The electronic transitions were analyzed by visualizing the Natural Transition Orbitals (NTOs). Additionally, the HFLD method was applied to calculate the interaction energy, incorporating the aug-cc-pVDZ basis set along with the auxiliary basis set aug-cc-pVDZ/C aug-cc-pVTZ/JK under the RIJK approximation.[18] Atoms in Molecules (AIM) analysis was performed using AIMALL software.[19] The Multiwfn 3.8 software package was utilized to visualize the deformation density contour map, providing insights into electronic structure modifications.[20] while Natural Bond Orbital (NBO) analysis was conducted using NBO 7.0.10.[21] The intrinsic bond strength index (IBSI) analysis was performed using the independent gradient model (IGM) with IGMplot (Rev. 3.08) software, based on the wave function obtained from the M062-X method with the 6-31G** basis set.[22,23] Molecular electrostatic potential (MEP) analysis was used to explore the reactive sites between CD and IBU. The visualization process was performed using the Chemcraft package[24] and VMD software.[25]

RESULTS AND DISCUSSION

Synthesis and Characterization of CD and ICD

Figure-1a and 1b shows the FT-IR spectra of CD, IBU, and ICD complex, obtained from theoretical and experimental methods, respectively. In CD, -NH and -COOH groups were confirmed with experimental frequencies at 3628–3300 cm^{-1} and theoretical values at 3568 cm^{-1} (NH), 3708 cm^{-1} (COOH), and 3773 cm^{-1} (free OH). Experimentally, stretching vibrations of -NH and -OH merged (3628–3300 cm^{-1}) due to strong vibrational coupling, as observed in previous studies.[26,27] In IBU, theoretical carboxylic O-H and C=O stretching appeared at 3707 cm^{-1} and 1740 cm^{-1}, while experimental values were 3185–3447 cm^{-1} (O-H) and 1634 cm^{-1} (C=O). After CD-IBU interaction, forming ICD, the O-H stretching of CD shifted from 3708 cm^{-1} to 2919 cm^{-1}, indicating hydrogen bond formation. The IR spectra obtained using r^{2}SCAN-3c showed strong agreement with experimental data, supporting further DFT analyses, including AIM, deformation density, IBSI, NBO, MEP, and FMO.

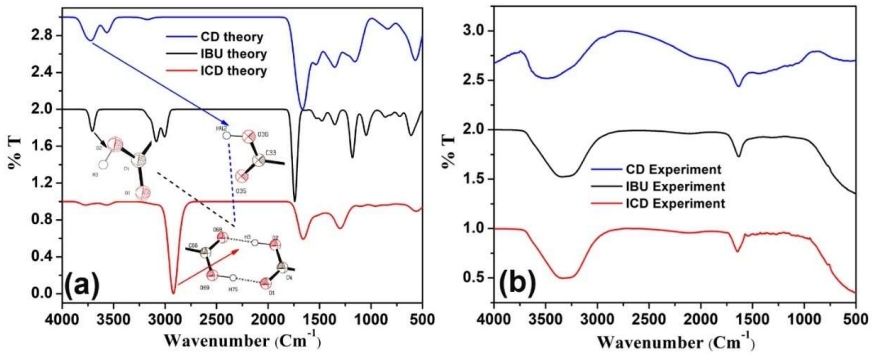

Fig.-1: FT-IR Spectrum of CD, IBU, and ICD Complex from (a) Theoretical and (b) Experimental Method

Figure-2a shows the electronic spectra of ICD in water, recorded to analyze optical properties. The absorption peak begins at 533 nm, two peaks appear at 260 nm and 323 nm, attributed to $\pi \rightarrow \pi^*$ and $n \rightarrow \pi^*$ transitions for C=C and C=O bonds, respectively. Theoretical UV spectra were computed using TD-DFT (CAM-B3LYP/Def2-TZVP) with CPCM (water) and compared with experimental results (Fig.-2a, red). Natural Transition Orbitals (NTOs) were also analyzed, revealing $\pi \rightarrow \pi^*$ and $n \rightarrow \pi^*$ transitions (Fig.-2a, inset). These transitions primarily involve the ICD ring and functional group lone pairs, with excitations occurring between HOMO-LUMO and HOMO-1-LUMO+1 energy levels.

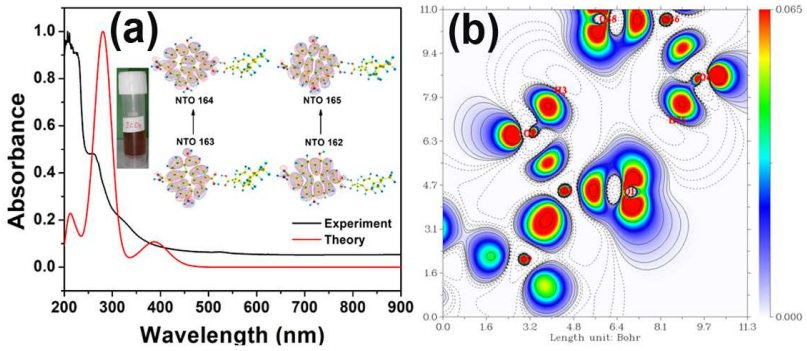

Fig.-2: (a) Experimental (black) and Theoretical (red) UV-Vis Spectra of ICD, (b) Deformation Density Image of ICD from the r^{2}SCAN-3c

Hartree-Fock Method with London Dispersion Corrections (HFLD) Analysis

HFLD is a first-principles method for analyzing non-covalent interactions in large molecular systems. The interaction energy of the ICD complex was calculated to be -105.107 kcal/mol using the aug-cc-pVDZ basis set and the RIJK approximation

Geometrical Analysis of CD, IBU, and ICD

The molecular structure of IBU was initially optimized (Fig.-3a) using the r^{2}SCAN-3c method. The geometric parameters of IBU (Table-1) closely matched the experimental data[28] (CCDC No: 2056854).

Table-1: Bond Length of IBU Calculated from Experimental[28] and DFT Method

Bond length (Å)	Exp	DFT	Bond length (Å)	Exp	DFT
C29-H32	1.060	1.095	C16-C17	1.387	1.400
C29-H31	1.070	1.096	C14-C16	1.383	1.396
C29-H30	1.058	1.098	C14-H15	1.083	1.088
C25-H33	1.056	1.096	C12-C14	1.373	1.393
C25-H27	1.059	1.096	C12-H13	1.083	1.088
C25-H26	1.059	1.097	C11-C19	1.385	1.399
C24-C29	1.503	1.528	C11-C12	1.389	1.395
C24-H28	1.101	1.101	C9-C11	1.529	1.523
C24-C25	1.522	1.529	C9-H10	1.097	1.095
C21-C24	1.495	1.544	C5-C9	1.519	1.532
C21-H23	1.094	1.098	C5-H8	1.068	1.094
C21-H22	1.092	1.098	C5-H7	1.07	1.092
C19-H20	1.083	1.087	C5-H6	1.056	1.094
C17-C19	1.388	1.390	C4-C9	1.539	1.519
C17-H18	1.084	1.088	O2-C4	1.253	1.346
C16-C21	1.513	1.505	O2-H3	0.968	0.973
			O1-C4	1.259	1.216

Table-2: Selected Bond Lengths of CD, IBU, and ICD from DFT Method

Bonds in ICD and IBU	IBU	ICD	CD	Bonds in CD
O2-H3	0.973	1.012	-	-
C4-O2	1.346	1.317	-	-
C4-O1	1.216	1.235	-	-
C4-C9	1.519	1.515	-	-
C66-O68	-	1.237	1.218	C33-035
C66-O69	-	1.320	1.348	C33-036
O69-H75	-	1.014	0.973	O36-H42
C66-C52	-	1.484	1.487	C33-C19
068-H3	-	1.616	-	-
O1-H75	-	1.612	-	-

This strong correlation emphasizes the reliability of the r^{2}SCAN-3c method in predicting molecular geometries, showing an accuracy comparable to or even exceeding other hybrid density functional

approximations.[14] After validating the accuracy of the r²SCAN-3c method, the same method was employed to investigate the interaction between IBU and CD (Fig.-3b).

Figure-3c shows the energy-minimized structure of the ICD. Table-2 lists the selected geometrical parameters of the CD, IBU, and ICD. Bond length O2-H3 (0.973 Å) and C4-O1 (1.216 Å) in IBU are increased to 1.012 Å and 1.235Å, after interaction with CD. Additionally, the bond length of C4-O2 in IBU decreased from 1.346 Å to 1.317 Å. Similarly, in CD, the bond lengths of C33-O35 and O36-H42 increased, whereas the C33-O36 bond length decreases in the ICD complex. The observed changes in the bond lengths indicate that hydrogen bond formation significantly influences the structural properties of both CD and IBU. The elongation of O2-H3, C4-O1, C33-O35, and O36-H42 suggests bond weakening due to interaction with CD, whereas the shortening of C4-O2 implies increased bond strength, likely due to electronic delocalization. These modifications highlight the role of hydrogen bonding in stabilizing the ICD complexes.

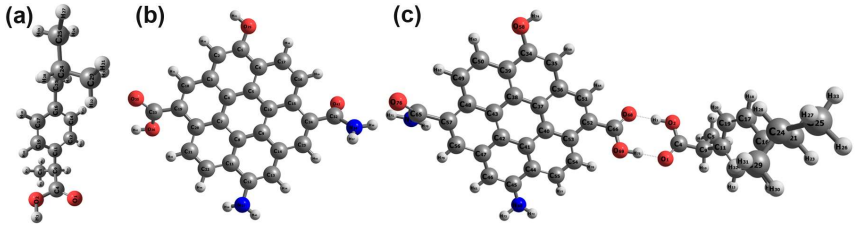

Fig.-3: Energy-Optimized Structure of (a) IBU, (b) CD, and (C) ICD at r²SCAN-3c Method

AIM analysis

Bader's Atoms in Molecules (AIM) theory was employed to characterize the nature of molecular interactions.[29] The selected bond topological parameters for CD, IBU, and ICD, calculated using the r²SCAN-3C method, are summarized in Table-3. The molecular graph of ICD is shown in Fig.-4a, and the Laplacian of electron density in Fig.-4b, providing a detailed topological analysis of interactions, bonding type, and electron density distribution.

Table-3: Selected Bond Topological Parameters of IBU, CD, and ICD

	Bonds	$\rho_{bcp}(r)^a$	$\nabla^2\rho_{bcp}(r)^b$	$\lambda_1{}^b$	$\lambda_2{}^b$	$\lambda_3{}^b$	ε	$G(r)^c$	$V(r)^c$	$H(r)^c$
IBU	O2-H3	0.3533	-2.0576	-1.8109	-1.7809	1.5341	0.0168	0.0691	-0.6527	-0.5835
	O1-C4	0.4041	0.3530	-1.0749	-0.9705	2.3984	0.1076	0.7624	-1.4366	-0.6742
	O2-C4	0.2972	-0.2396	-0.6591	-0.6202	1.0397	0.0626	0.4011	-0.8620	-0.4610
CD	O36-H42	0.3461	-1.9185	-1.7930	-1.7633	1.6377	0.0168	0.0638	-0.6073	-0.5435
	C33-O35	0.4076	-0.1580	-1.0811	-0.9780	1.9012	0.1054	0.6641	-1.3677	-0.7036
	C33-O36	0.3014	-0.5861	-0.6613	-0.6437	0.7189	0.0272	0.3040	-0.7545	-0.4505
ICD	O1-H75	0.0564	0.1377	-0.1072	-0.1056	0.3505	0.0154	0.0427	-0.0511	-0.0083
	H3-O68	0.0556	0.1384	-0.1049	-0.1034	0.3467	0.0150	0.0424	-0.0502	-0.0078
	C66-O68	0.3891	-0.2727	-1.0074	-0.9240	1.6587	0.0902	0.5925	-1.2531	-0.6607
	C66-O69	0.3215	-0.5539	-0.7388	-0.7115	0.8964	0.0385	0.3638	-0.8660	-0.5023
	O69-H75	0.3005	-1.5152	-1.5004	-1.4794	1.4646	0.0142	0.0692	-0.5172	-0.4480
	O2-H3	0.3024	-1.5327	-1.5135	-1.4934	1.4742	0.0134	0.0691	-0.5213	-0.4522
	O1-C4	0.3903	-0.2379	-1.0104	-0.9389	1.7114	0.0762	0.6032	-1.2660	-0.6627
	O2-C4	0.3223	-0.5252	-0.7319	-0.7222	0.9290	0.0134	0.3736	-0.8785	-0.5049

[a] The electron density $\rho_{bcp}(r)$ (eBohr^{-3}), [b]Laplacian of electron density $\nabla^2\rho bcp(r)$ (eBohr^{-5}), [c]Energy density (HBohr^{-3})

Topological parameters at bond critical points (BCPs) confirm non-covalent interactions in the ICD complex, specifically hydrogen bonding between O1-H75 and H3-O68. This is supported by low electron densities (ρ) of O1-H75 (0.0564 eBohr^{-3}) and H3-O68 (0.0556 eBohr^{-3}), along with positive values of $\nabla^2\rho(r)$ for O1-H75 (0.1377 eBohr^{-5}) and H3-O68 (0.1384 eBohr^{-5}). The eigenvalues ($\lambda1 < 0, \lambda2 < 0, \lambda3 > 0$) and $-G(r_c)/V(r_c)$ ratio above 0.8 further validate these interactions. The near-zero ellipticity (ε) value indicates stability. As a result of hydrogen bonding, the electron densities of the O2-H3 (0.3533 eBohr^{-3}) and O1-

C4 (0.4041 eBohr^{-3}) bonds in IBU decreased to 0.3024 and 0.3903 eBohr^{-3}. Similarly, O36-H42 (0.3461 eBohr^{-3}) and C33-O35 (0.4076 eBohr^{-3}) bonds in CD decrease to 0.3005 and 0.3891 eBohr^{-3}, respectively. This reduction in electron density in CD and IBU leads to bond elongation and a corresponding decrease in bond strength, as confirmed by the geometrical and IBSI analyses.

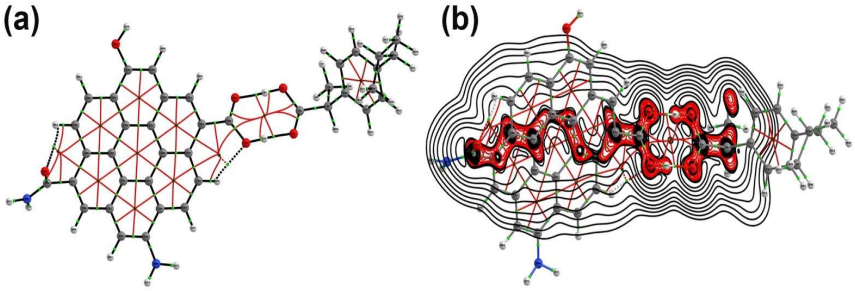

Fig.-4: (a) Critical Point Image of the ICD Molecules. (b) Laplacian of Electron Density of ICD Derived from Wave Function Calculated at r^{2}SCAN-3c Method

Deformation density (ρdef) analysis, a key tool for studying non-covalent interactions, highlights charge redistribution. Figure-2b illustrates electron density deformation in the ICD complex, showing hydrogen bonding effects between O66–H3 and O1–H75. Red contours indicate areas of increased electron concentration due to intermolecular interactions.

Molecular Electrostatic Potential (MEP)

MEP serves as a valuable tool for visualizing charge distribution within molecules, allowing the identification of electron-rich and electron-deficient regions. Figure-5c displays the isosurface image of ICD, while the isolated MEP image of IBU (Fig.-5a) and CD (Fig.-5b) highlights the charge distribution. The positive charge density around the O-H bond appears in blue, whereas the oxygen atom exhibits a negative charge density in red. These distinctions help identify the nucleophilic and electrophilic reactive sites on IBU and CD, respectively. The interactions between these regions facilitate hydrogen bond formation, potentially driving various molecular transformations. These transformations can be further analyzed using geometrical parameters, AIM, NBO, and IBSI analyses.

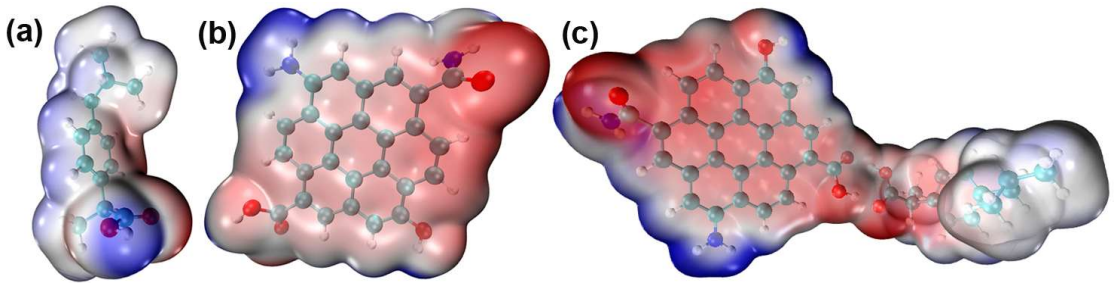

Fig.-5: Isosurface image of the electrostatic potential of (a) IBU, (b) CD, and (c) ICD at r^{2}SCAN-3c

Independent Gradient Model (IGM) Analysis

The IGM-δg method is a tool for analyzing and quantifying molecular associations by assessing electron density topology derived from AIM analysis. It specifically focuses on the gradient of the electron density (∇ρ), allowing for the identification of both intra- and intermolecular interactions. Using the δg descriptor, this approach provides valuable insights into a range of interactions, including covalent, hydrogen bonds, transition metal, and van der Waals interactions.[30] The interaction between CD and IBU was primarily driven by hydrogen bonding at O1-H75 and H3-O68, with IBSI values of 1.612 and 1.616, respectively. These values indicate a significant bond strength, suggesting a stable interaction. Additionally, the IGM profile (Fig.-6a), with a δg value of 0.13 a.u., reinforces the presence of a robust hydrogen bond, emphasizing its role in the overall molecular interaction. Together, IBSI and IGM analyses illustrate how

these interactions contribute to enhanced drug stability and bioavailability, offering potential benefits for drug delivery systems and improving therapeutic efficacy in various biomedical contexts.

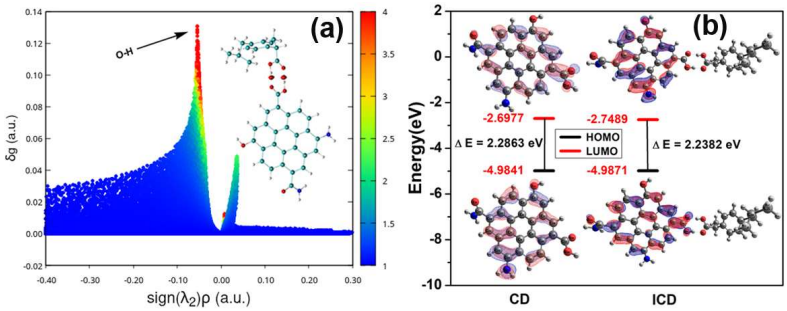

Fig.-6: (a) IGM- δg Signature in ICD Molecule (b) HOMO and LUMO Orbital Structure of CD and ICD

Table-4: Selected IBSI Value of ICD

	Bond	*d* (Å)	δg	IBSI	PDA	Direction of asymmetry
ICD	O1-H75	1.612	0.310	0.166	218.8	H75-->O1
	H3-O68	1.616	0.303	0.161	218.1	O68<--H3
	C66-O68	1.237	2.161	1.965	89.2	C66-->O68
	C66-O69	1.320	1.867	1.492	81.8	C66-->O69
	O69-H75	1.014	0.840	1.138	346.1	O69<--H75
	O2-H3	1.012	0.845	1.149	346.3	H3-->O2
	O1-C4	1.235	2.157	1.969	89.9	O1<--C4
	O2-C4	1.317	1.857	1.490	82.5	O2<--C4

The intrinsic bond strength index (IBSI) quantitatively measures bond strength within a molecule, providing a numerical measure of bond stability and offering insights into molecular interactions.[30] Table-4 presents selected IBSI values for ICD. These values help to assess the strength of newly formed hydrogen bonds and their impact on the surrounding hydrogen bond environments. AIM analysis confirmed that CD and IBU were linked through non-covalent interactions involving O1–H75 and H3–O68 bonds. To quantify the strength of these interactions, IBSI analysis was performed, resulting in values of 0.166 and 0.161, respectively. For CD, the IBSI values for O36–H42 and C33–O35 were 1.365 and 2.112, respectively. However, after interaction with IBU, these values decrease to 1.138 and 1.965, respectively. Similarly, the IBSI values for O2–H3 and O1–C4 in IBU also decreased after interaction with CD, indicating a reduction in the bond strength. Conversely, the bond strength of C33–O36 in CD and C4–O2 in IBU increased with respect to the ICD complex, highlighting the structural changes induced by the interaction within the molecular framework.

Natural Bond Orbital (NBO) Analysis

NBO analysis, developed by Frank Weinhold[31]offers detailed insights into electron distribution and interactions within and between molecules. This method is especially useful for examining the bonding characteristics, charge transfer phenomena, and electronic structure. It has become a widely used tool for investigating the hydrogen bonding, charge delocalization, and the stability of molecular systems. The selected NBO orbital is illustrated in Fig.-7.

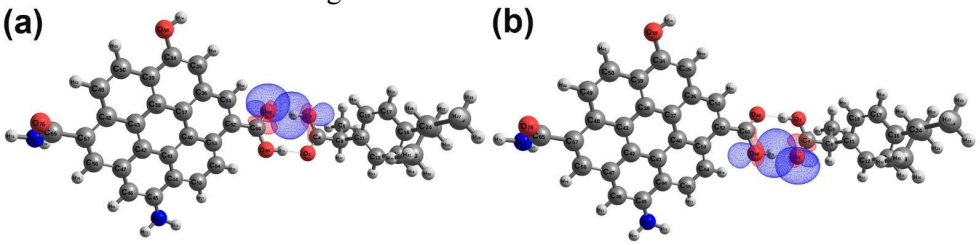

Fig.-7: Selective NBOs O-H-O Interactions in ICD

The oxygen atom (O1) of IBU donates its lone pair (n2, occupancy: 1.833) to the hydrogen atom (H75) of the CD (acceptor, LV1 occupancy: 0.4646). Similarly, the oxygen atom (O68) of CD donates its lone pair (n2, occupancy: 1.833) to the hydrogen atom (H3) of IBU (acceptor, LV1 occupancy: 0.4644). The stabilization energy of 56.68 and 54.99 kcal/mol suggests a strong interaction, which is further supported by the relatively small energy gap (0.43 a.u.) between the donor and acceptor orbitals. Additionally, the Fock matrix element (0.139 a.u.) indicates a reasonable overlap between these orbitals, contributing to the interaction strength. This interaction model could provide valuable insight into how IBU molecules bind to or interact with CD, potentially aiding drug formulation or delivery research involving CD.

Frontier Molecular Orbital Analysis

Figure-6b presents the values of the HOMO and LUMO energies, along with their energy differences, for CD and ICD. These data illustrate how the electronic properties of the CD are affected by the interaction, highlighting the changes in their stability and reactivity. The CD has a HOMO-LUMO band gap of 2.2863 eV, which shifts to 2.2382 eV upon interaction with IBU. This change suggests enhanced electronic stability while maintaining the reactivity. Although the new band gap remains lower than that of the drug, it reflects a balance between stability and reactivity. This adjustment may improve the suitability of CD for drug delivery, for which both properties are essential.

CONCLUSION

We validated the structures of CD and ICD using FTIR and UV-Vis spectra, comparing results with DFT calculations. AIM analysis confirmed non-covalent interactions, while IBSI evaluated interaction strength, and IGM quantified them. The interaction energy was analyzed using the accurate HFLD method. Electron and deformation density mapping identified interaction sites and bonding characteristics. FMO analysis highlighted electronic properties and reactivity, while NBO analysis revealed charge delocalization and stabilization effects. MEP analysis identified potential interaction sites, further supporting observed non-covalent interactions. This study provides essential insights for designing carbon dot-based drug delivery systems with computational and spectroscopic validation.

ACKNOWLEDGMENTS

Thangavel Subramani and Karthik Krishnasamy express their gratitude to the Bioinformatics Resources and Applications Facility (BRAF), C-DAC, Pune, for supporting this study with computational resources.

CONFLICT OF INTERESTS

The authors declare that there is no conflict of interest.

AUTHOR CONTRIBUTIONS

The present work is related to *SDG-3: Good Health and Well-being*. All the authors contributed significantly to this manuscript, participated in reviewing/editing and approved the final draft for publication. The research profile of the authors can be verified from their ORCID IDs, given below:

K. Karthik http://orchid.org/0000-0002-5131-2982
S. Thangavel http://orchid.org/0000-0002-3315-6605

REFERENCES

1. C. Kang, Y. Huang, H. Yang, X. F. Yan and Z. P. Chen, *Nanomaterials*, **10(11)**, 1(2020), https://doi.org/10.3390/nano10112316
2. R. Das, R. Bandyopadhyay and P. Pramanik, *Materials Today Chemistry*, **8**, 96(2018), https://doi.org/10.1016/j.mtchem.2018.03.003
3. C. L. Li, C. C. Huang, A. P. Periasamy, P. Roy, W. C. Wu, C. L. Hsu and H. T. Chang, *RSC Advances*, **5(3)**, 2285(2015), https://doi.org/10.1039/C4RA11704B
4. W. Li, Y. Zheng, H. Zhang, Z. Liu, W. Su, S. Chen and B. Lei, *ACS Applied Materials and Interfaces,* **8(31)**, 19939(2016), https://doi.org/10.1021/acsami.6b07268

5. S. Y. Lim, W. Shen and Z. Gao, *Chemical Society Reviews*, **44(1)**, 362(2015), https://doi.org/10.1039/C4CS00269E
6. S. N. Baker and G. A. Baker, *Angewandte Chemie International Edition,* **49(38)**, 6726(2010), https://doi.org/10.1002/anie.200906623
7. E. Janus, P. Ossowicz, J, Klebeko, A. Nowak, W. Duchnik, Ł. Kucharski and A. Klimowicz, *RSC Advances*, **10(13)**, 7570(2020), https://doi.org/10.1039/D0RA00100G
8. Y. Zhang, Y. Gao, X. Wen and H. Ma, *Asian Journal of Pharmaceutical Sciences*, **9(2)**, 65(2014), https://doi.org/10.1016/j.ajps.2013.12.006
9. Y. M. Chen and N. Rodríguez-Hornedo, *Crystal Growth and Design*, **18(3)**, 1358(2018), https://doi.org/10.1021/acs.cgd.7b01206
10. F. A. Maulvi, S. J. Dalwadi, V. T. Thakkar, T. G. Soni, M. C. Gohel and T. R. Gandhi, *Powder Technology*, **207(1)**, 47(2011), https://doi.org/10.1016/j.powtec.2010.10.009
11. S. Koranne, J. F. Krzyzaniak, S. Luthra, K. K. Arora, and R. Suryanarayanan, *Crystal Growth and Design*, **19(2)**, 868(2019), https://doi.org/10.1021/acs.cgd.8b01430
12. X. Dong, W. Liang, M. J. Meziani, Y. P. Sun and L. Yang, *Theranostics*, **10(2)**, 671(2020), https://doi.org/10.7150/thno.39863
13. G. G. Naik, M. B. Alam, V. Pandey,D. Mohapatra, P. K. Dubey, A. S. Parmar and A. N. Sahu, *Journal of Fluorescence*, **30(2)**, 407(2020), https://doi.org/10.1007/s10895-020-02515-0
14. S. Grimme, A. Hansen, S. Ehlert and J. M. Mewes, *The Journal of Chemical Physics,* **154(6)**, 2021, https://doi.org/10.1063/5.0040021
15. T. Gasevic, J. B. Stückrath, S. Grimme, and M. Bursch, *The Journal of Chemical Physics A*, **126(23)**, 3826(2022), https://doi.org/10.1021/acs.jpca.2c02951
16. F. Neese, *Wiley Interdisciplinary Reviews: Computational Molecular Science*, ***12*(5)**, p.e1606(2022), https://doi.org/10.1002/wcms.1606
17. T. Yanai, D. P. Tew and N. C. Handy, *Chemical Physics Letters*, **393(1)**, 51(2004), https://doi.org/10.1016/j.cplett.2004.06.011
18. A. Altun, F. Neese and G. Bistoni, *Journal of Chemical Theory and Computation*, **15(11)**, 5894(2019), https://doi.org/10.1021/acs.jctc.9b00425
19. T. A. Keith, "Aimall (Version 19.10. 12), todd a. keith, tk gristmill software: Overland park ks (2019)," *URL http//aim. tkgristmill. com*.
20. T. Lu and F. Chen, *Journal of Computational Chemistry,* **33(5)**, 580(2012), https://doi.org/10.1002/jcc.22885
21. E. D. Glendening, C. R. Landis and F. Weinhold, *Journal of Computational Chemistry,* **40(25)**, 2234(2019), https://doi.org/10.1002/jcc.25873
22. C. Lefebvre, H. Khartabil and E. Hénon, *Physical Chemistry Chemical Physics,* **25(16)**, 11398(2023), https://doi.org/10.1039/D2CP02839E
23. C. Lefebvre, J. Klein, H. Khartabil, J. C. Boisson and E. Hénon, J*ournal of Computational Chemistry,* **44(20)**, 1750(2023), https://doi.org/10.1002/jcc.27123
24. G. A. Andrienko, "Chemcraft-graphical software for visualization of quantum chemistry computations," *See* https//www.chemcraftprog.com, 2010
25. W. Humphrey, A. Dalke and K. Schulten, *Journal of Molecular Graphics,* **14(1)**, 33(1996), https://doi.org/10.1016/0263-7855(96)00018-5
26. K. Patir and S. K. Gogoi, *Nanoscale Advances*, **1(2)**, 592(2019), https://doi.org/10.1039/C8NA00080H
27. C. J. Reckmeier, J. Schneider, Y. Xiong, J. Häusler, P. Kasák, W. Schnick, and A. L. Rogach, *Chemistry of Materials,* **29(24)**, 10352(2017), https://doi.org/10.1021/acs.chemmater.7b03344
28. O. Al Rahal, P. A. Williams, C. E. Hughes, B. M. Kariuki and K. D. M. Harris, *Crystal Growth and Design,* **21(4)**, 2498(2021), https://doi.org/10.1021/acs.cgd.1c00160
29. S. J. Grabowski, *Chemical Review,* **111(4)**, 2597(2011), https://doi.org/10.1021/cr800346f
30. J. Klein, H. Khartabil, J. C. Boisson, J. Contreras-Garciá, J. P. Piquemal, and E. Hénon, *Journal of Physical Chemistry A*, **124(9)**, 1850(2020), https://doi.org/10.1021/acs.jpca.9b09845
31. F. Weinhold, C. R. Landis and E. D. Glendening, *International Reviews in Physical Chemistry,* **35(3)**, 399(2016), https://doi.org/10.1080/0144235X.2016.1192262

[RJC-9286/2025]